Effects of pre-compression deformation on nanoindentation response of $Zr_{65}Cu_{15}Al_{10}Ni_{10}$ bulk metallic glass

Hu Huang [a], Jiliang Zhang [b], Chan-Hung Shek [b], Jiwang Yan [a], *

[a] Department of Mechanical Engineering, Faculty of Science and Technology, Keio University, Hiyoshi 3-14-1, Kohoku-ku, Yokohama 223-8522, Japan
[b] Department of Physics and Materials Science, City University of Hong Kong, Kowloon Tong, Hong Kong, China

A B S T R A C T

Nanoindentation experiments were conducted on $Zr_{65}Cu_{15}Al_{10}Ni_{10}$ bulk metallic glass samples with pre-compression deformation (PCD) under various conditions. By analyzing indentation hardness, residual morphology, pile-up, and serrated flow, the effects of PCD on nanoindentation response were comparatively investigated. Experimental results indicate that 9 kN PCD induced remarkable decrease of indentation hardness, i.e. softening of the material, while for the 18 kN and 25 kN PCD samples, hardness values very close to that of the as cast sample were obtained. Furthermore, PCD also changed the mechanical heterogeneity, i.e., distribution of soft and hard regions in the bulk metallic glass. Residual morphologies and load-displacement curves of the 9 kN and 18 kN PCD samples showed opposite features in aspects of macroscopic shear bands, pile-up width, pile-up height, and serrated flows, suggesting different plastic flows during nanoindentation. To rationalize these phenomena, a competing mechanism between shear bands and compressive residual stress was discussed.

© 2016 Elsevier B.V. All rights reserved.

1. Introduction

Taking advantages of excellent mechanical properties such as high hardness, large elastic limit, and superior resistance to wear and corrosion, bulk metallic glasses (BMGs) have been regarded as emerging structural materials. However, due to absence of dislocations and grain boundaries, BMGs generally deform via individual shear banding process, and show very limited microscopic plasticity followed by catastrophic failure [1], which significantly limits their applications. Hence, deformation mechanisms of BMGs under external loads are attracting continuous attentions [2–7]. Because of high measuring resolution, small probing volume, and good compatibility for brittle materials, nanoindentation has been widely used to investigate shear banding, creep, and plastic deformation of various types of BMGs in micro-/nano-scales [8–14].

The nanoindentation of BMGs shows three typical characters: serrated flows, semi-circular shear bands and pile-ups [12,14–18], which are directly related to plastic deformation of BMGs. Previous results indicated that many factors such as indentation rates [15],

indenter geometry [17,18], residual stresses [19], and pre-deformation [20,21] could change these characters. Schuh et al. [15] reported that low indentation rates promoted serrated flows while high rates strongly suppressed serrated flows. Yoo et al. [17,18] found that the cube-corner indenter with a small face angle promoted more remarkable serrated flows and macroscopic shear bands compared with the Berkovich indenter. Haag et al. [19] suggested that tension residual stress suppressed the pile-up, increased the serrated width but induced relatively smooth residual indents, while compressive residual stress promoted the pile-up and macroscopic shear bands. Jiang et al. [20] reported that macroscopic shear bands and serrated flows were hindered by cold rolling and laser shock peening [20–23]. In this study, by comparatively investigating the nanoindentation response of $Zr_{65}Cu_{15}Al_{10}Ni_{10}$ BMGs after various pre-compression deformations (PCDs), an inconsistent relationship between macroscopic shear bands and serrated flows, i.e. conspicuous macroscopic shear bands corresponding to non-serrated flows while smooth indent corresponding to promoted serrated flows, will be reported and discussed.

2. Material and experiments

Alloy ingots with a nominal composition of $Zr_{65}Cu_{15}Al_{10}Ni_{10}$ in

* Corresponding author.
  E-mail address: yan@mech.keio.ac.jp (J. Yan).

atomic percent were produced by arc-melting the mixtures of high-purity (99.9%) Zr, Cu, Al, and Ni elements in a Ti-gettered high-purity argon atmosphere. Then, they were re-melted three times for homogeneity. Glassy rods with the diameter of 2 mm were fabricated by a water-chilled copper mold suction casting setup. After that, the rods were cut into shorter cylinders with a diameter of 2 mm and length of 2 mm by a low speed diamond saw with oil cooling, and then washed by methanol in an ultrasonic cleaner. PCD was carried out on three of these cylinders under the same strain rate of 1×10^{-3}/s but different compression loads, 9 kN, 18 kN and 25 kN, resulting in deformation of ~ 30%, 55% and 65%. Samples for nanoindentation tests were embedded by epoxy with the thickness of 3 mm, leaving the top surface of the PCD samples exposure, and then they were polished to be mirror surfaces.

Lateral morphologies of the PCD samples were observed by a JEOL JSM820 scanning electron microscope (JEOL Ltd., Japan). An X-ray diffractometer (XRD, D8 Discover, Bruker) was used to verify the amorphous feature of the samples before and after PCD. Nanoindentation tests were performed on the top surface of the PCD samples using an ENT-1100 nanoindentation instrument (Elionix Inc., Japan) with a Berkovich indenter at room temperature. To reduce effects of sample preparation and surface roughness, a large indentation load of 1000 mN was used, producing an indentation depth of ~ 2.9 μm. For each samples, 100 indents (10×10 array) were reduplicated to obtain reliable indentation data. Distance between adjacent indents was 50 μm to avoid the boundary effect. For all indents, a same loading/unloading rate (10 mN/s) and holding time at the maximum indentation load (30 s) were selected. Residual indent morphologies were measured by a 3D laser scanning microscope (VK-9700, Keyence).

3. Results and discussion

Fig. 1 presents the lateral morphologies of the PCD samples under different compression loads. Profuse shear bands crossing the whole samples were produced although their distribution is still inhomogeneous. With the increase of the PCD load, main shear bands changed their orientations. For the 9 kN PCD sample, the angle of main shear band with the compression direction is about 48°, and it increased gradually up to 69° for the 25 kN PCD sample. This angle change of main shear band mainly results from the geometric constraint (the aspect ratio of the sample is 1), leading to remarkable height change of the sample with the increase of compression loads.

Fig. 2 presents XRD patterns of the as cast and PCD samples, and only a broad hump can be seen in all XRD patterns, indicating no obvious crystallization in these samples.

According to the Oliver and Pharr method [24], Fig. 3(a) gives the average indentation hardness of these samples. Obviously, the 9 kN PCD sample has the smallest hardness of 4.24 GPa on average, while the further increased PCD load hardens samples, e.g. 5.09 GPa for the 18 kN PCD sample and 4.90 GPa for the 25 kN PCD sample. Compared with significantly softening of the 9 kN PCD sample, samples deformed with a large load show a hardness very close to
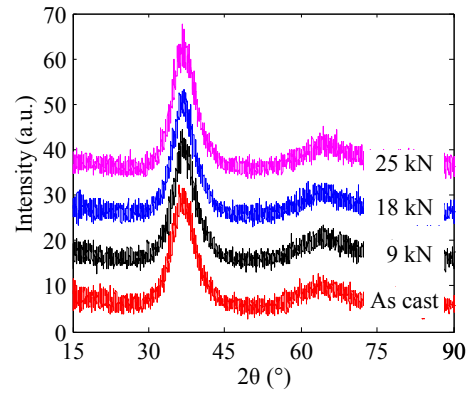

Fig. 2. XRD patterns of the as cast and PCD samples.
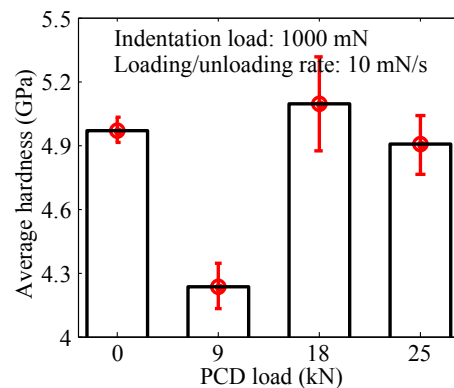

Fig. 3. Average indentation hardness vs. PCD load.

that of the as cast sample (4.97 GPa).

Results in Fig. 3 indicate that with the increase of the PCD load, the average hardness initially decreases and then increases to the hardness comparable to that of the as cast BMG. Similar hardness evolution was previously reported for the $Zr_{58.5}Cu_{15.6}Ni_{12.8}Al_{10.3}Nb_{2.8}$ BMG during cold rolling [22]. To explain this evolution, authors [22] proposed a competing mechanism between shear band generation and residual stress, which can also be used to explain the hardness evolution in Fig. 3. With the increase of the PCD load, evolution of shear bands and compressive residual stress happened, especially for these samples with an aspect ratio of 1. The orientation change of main shear band in Fig. 1 further confirms the evolution of shear bands. Furthermore, with the orientation change of main shear band, new shear bands should nucleate to carry the subsequent plastic strain [25]. Previous research [9] by nanoindentation mapping near a single shear band indicates that compared to the surrounding amorphous matrix, shear bands are relatively soft with reduced hardness. Thus, the hardness decrease for the 9 kN PCD sample is derived to be the contribution of pre-
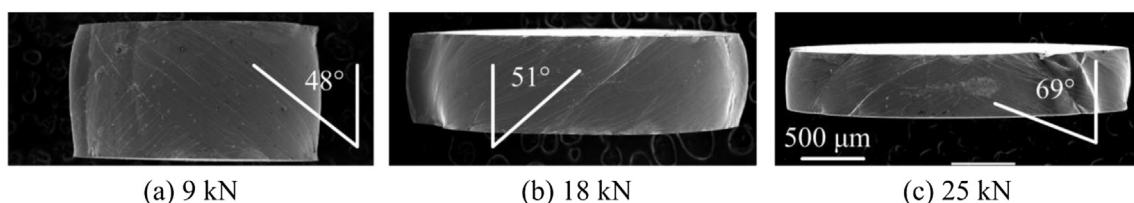

Fig. 1. Lateral morphologies of the PCD samples under different compression loads: (a) 9 kN, (b) 18 kN, and (c) 25 kN. Orientations of main shear band are illustrated by angles.

existing shear bands formed during the PCD. With the increase of the PCD load to 18 kN and 25 kN, shear bands further evolved, and the compressive residual stress was developed to be the dominated factor that affects the hardness. Previous research [10,19,26] indicates that compressive residual stress has small impact on the indentation hardness of BMGs, and thus hardness values very close to that of the as cast sample were obtained for the 18 kN and 25 kN PCD samples.

In Fig. 3, it is also noted that the PCD yields wider distribution of hardness and likely leads to larger mechanical heterogeneity. To further address this, Fig. 4 shows the hardness mappings in the measuring regions (10 × 10 array with an interval of 50 μm). Relative change of the indentation hardness against the average makes it more evident as shown in the mappings in Fig. 5. It is noted that only one frame shows a much larger hardness in the as cast sample in Fig. 4(a), which is very likely due to the artificial error. In Fig. 4(b), mechanical heterogeneity is enhanced in the 9 kN PCD sample. When the PCD load increases to 18 kN, the hard regions are more concentrated and they can be easily distinguished with the soft regions. However, hardness distribution becomes relatively homogeneous again in the 25 kN PCD sample. As mentioned above, shear bands are soft regions, but their propagation is spatially varied [9]. Thus, interlaced shear bands could be induced inside and on the lateral surface of the PCD samples, which may be the reason leading to mechanical heterogeneity in the PCD samples. When nanoindentation is performed on or near the shear band, reduced hardness will be obtained and a soft region is identified. In contrast, when nanoindentation is performed on position between two shear bands, a hardness value close to that of the as cast BMG is obtained, i.e. hard region. The soft and hard regions are evolved accompanying with evolution of shear bands which is mainly determined by the PCD load, leading to various hardness distributions in Figs. 4 and 5.

It is agreed [27] that mechanical heterogeneity can affect plasticity of BMGs significantly. To study effects of PCD induced mechanical heterogeneity on plastic deformation during nanoindentation, residual indent morphologies are also studied in Fig. 6(a)–(d). The possibility to observe macroscopic shear bands around indents is plotted in Fig. 6(e). Macroscopic shear bands always appear around all indents in the as cast samples, but there is no visible macroscopic shear bands in the 9 kN PCD sample. Fig. 6(f)–(i) show depth profiles along A–A′ cross-sections

Fig. 5. Relative change of indentation hardness against the average in the measuring regions for the samples after different PCDs: (a) as cast; (b) 9 kN; (c) 18 kN; (d) 25 kN.

corresponding to Fig. 6(a)–(d) respectively. Obviously, the pile-up heights of these four samples are in the following order: the 18 kN PCD sample > the as cast sample > the 25 kN PCD sample > the 9 kN PCD sample. Previous investigations indicate that the pile-up generally leads to overestimation of the hardness by the Oliver and Pharr method [28]. Thus, Meyer hardness (load/ projected area) is used to calculate the hardness based on the morphologies in Fig. 6(a)–(d). Projected areas of these four indents are obtained by measuring the projected contact lengths, and they are 200.09, 221.12, 177.36 and 201.81 μm², respectively. Thus, Meyer hardness corresponding to Fig. 6(a)–(d) are 4.99, 4.52, 5.63 and 4.95 GPa, respectively, while the estimated hardness by the Oliver and Pharr method are 4.98, 4.31, 5.47, 4.96 GPa respectively. At this point, hardness values obtained using these two methods are very close. In Fig. 6(f)–(i), the 18 kN PCD sample shows the smallest pile-up width followed by the as cast sample, while the 9 kN PCD sample shows the largest width. Pile-up with large height and small width means deformation localization [19]. So, from as cast sample to 9 kN PCD sample, the ZrCuNiAl BMG trends to deform from a discrete plastic flow to a nearly continuous plastic flow. With the increase of the PCD load to 18 kN, the plastic flow becomes discrete and highly localized again. When the PCD load further increases to 25 kN, the ZrCuNiAl BMG trends to continuously deform again with reduced macroscopic shear bands.

It is generally agreed that operations of shear bands including nucleation, propagation and arrest correspond to discrete displacement burst ("serrated flow") in the loading portion of the load-displacement curve in BMGs [1,15]. Different morphologies of macroscopic shear bands usually correspond to different serrated flows [17,18]. Fig. 7(a) gives load-displacement curves corresponding to residual indents in Fig. 6(a)–(d). A close view of the dotted zone is shown in Fig. 7(b). Conspicuous serrated flows appear in the loading portions of the as cast sample and the 9 kN PCD sample, while it is relatively smooth for the 18 kN and 25 kN PCD samples. To highlight this difference, the displacement difference changing with the indentation load is plotted in Fig. 7(c) according to the displacement difference method [29]. For a serrated flow in Fig. 7(b), the displacement difference first increases and then decreases, resulting in a sharp peak in Fig. 7(c). The peak height denotes the size of the serrated flow, corresponding to the burst displacement. Large peak height means big burst displacement during the serrated flow. Among these samples, both the as cast sample and the 9 kN PCD sample show more and higher peaks,
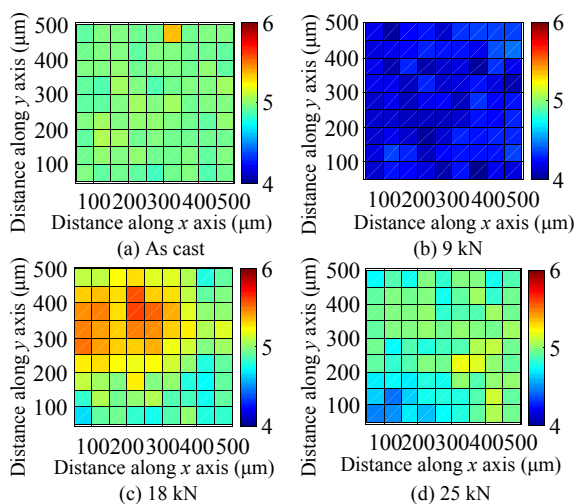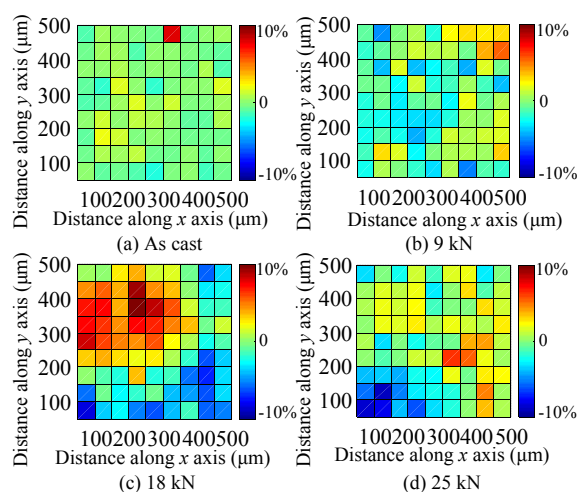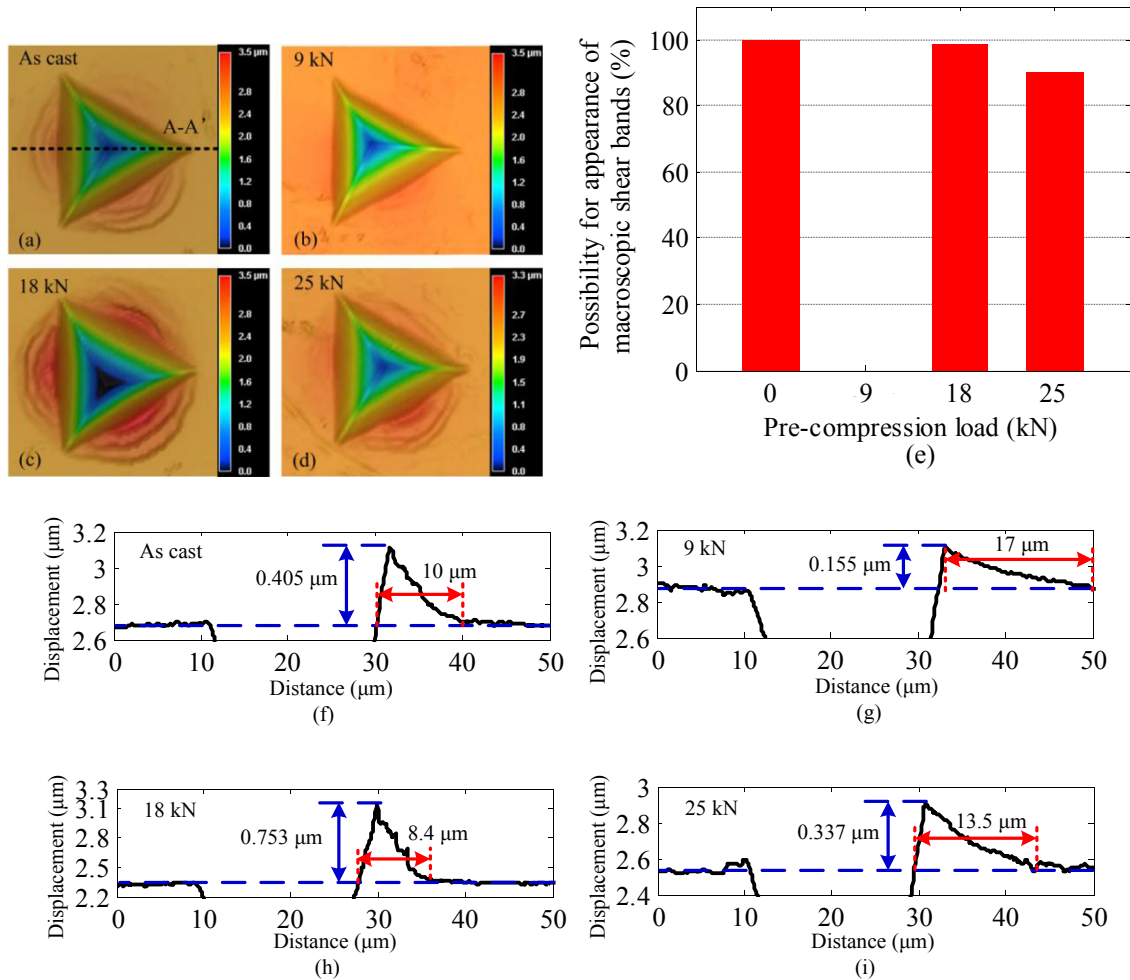

Fig. 4. Distribution of indentation hardness (Unit: GPa) in the measuring regions for the samples after different PCDs: (a) as cast; (b) 9 kN; (c) 18 kN; (d) 25 kN. One frame denotes one measuring point.

Fig. 6. Representative indent morphologies for the samples after different PCDs: (a) as cast; (b) 9 kN; (c) 18 kN and (d) 25 kN; (e) the possibility for appearance of macroscopic shear bands vs. the pre-compression load; A–A′ cross-sectional curves corresponding to Fig. 6(a)–(d): (f) as cast; (g) 9 kN; (h) 18 kN and (i) 25 kN.

while other samples especially the 18 kN PCD sample present a very smooth curve, suggestive of the strong suppression on the serrated flows. It should be noted that the phenomenon shown in Fig. 7 is observed in nearly all nanoindentation results.

It is generally reported that conspicuous macroscopic shear bands correspond to promoted serrated flows [16–18]. However, in the present work, a relatively smooth indent in Fig. 6(b) has been observed to promote serrated flows for the 9 kN PCD sample, while conspicuous macroscopic shear bands in Fig. 6(c) correspond to weakest serrated flows for the 18 kN PCD sample, suggesting different plastic flows during nanoindentation.

For the 9 kN PCD sample, the smooth indent without macroscopic shear bands as well as largest pile-up width implies continuous plastic flow on the top surface. So, there is nearly no nucleation and propagation of new shear bands on the top surface. However, conspicuous serrated flows in the loading portion suggest frequent operations of shear bands. Thus, the promoted serrated flows are derived to be resulted from operations of these pre-existing shear bands inside the sample formed during the 9 kN PCD. These pre-existing shear bands are soft regions [21], and the applied plastic strain during nanoindentation could be easily accommodated via propagation from these pre-existing shear bands, rather than nucleation of new shear bands on the top surface. Hence, reduced hardness, relatively smooth indent, largest pile-up width but promoted serrated flows were induced for the

9 kN PCD sample.

With regard to the 18 kN PCD sample, compressive residual stress was developed to be the dominated factor accompanying with evolution of shear bands. The hardness mapping shown in Fig. 5(c) with more concentrated distribution of hard and soft regions further confirms the evolution of shear bands. Compressive residual stress hindered the downward flow the BMG during nanoindentation [19], and the concentrated distribution of hard and soft regions also hindered the lateral flow of the BMG on the top surface. Thus, highly localized plastic deformation was induced with promoted pile-up height and conspicuous macroscopic shear bands.

The indentation behaviors (hardness, macroscopic shear band, pile-up, and serrated flow) of the 25 kN PCD sample show an intermediate status between the 9 kN and 18 kN PCD samples. Compared to the 18 kN PCD sample, a "recovery" phenomenon that a more homogeneous hardness distribution (shown in Fig. 5) and a lower but wider pile-up (shown in Fig. 6), seems to appear for the 25 kN PCD sample. Such "recovery" phenomenon reflects the evolution of the competing relationship between shear band generation and residual stress. The indentation hardness of the 25 kN PCD sample is very close to that of the as cast sample, suggesting that compressive residual stress played an important role during nanoindentation. On the other hand, the angle of main shear band increased from 51 to 69° in Fig. 1 when the PCD load increased from
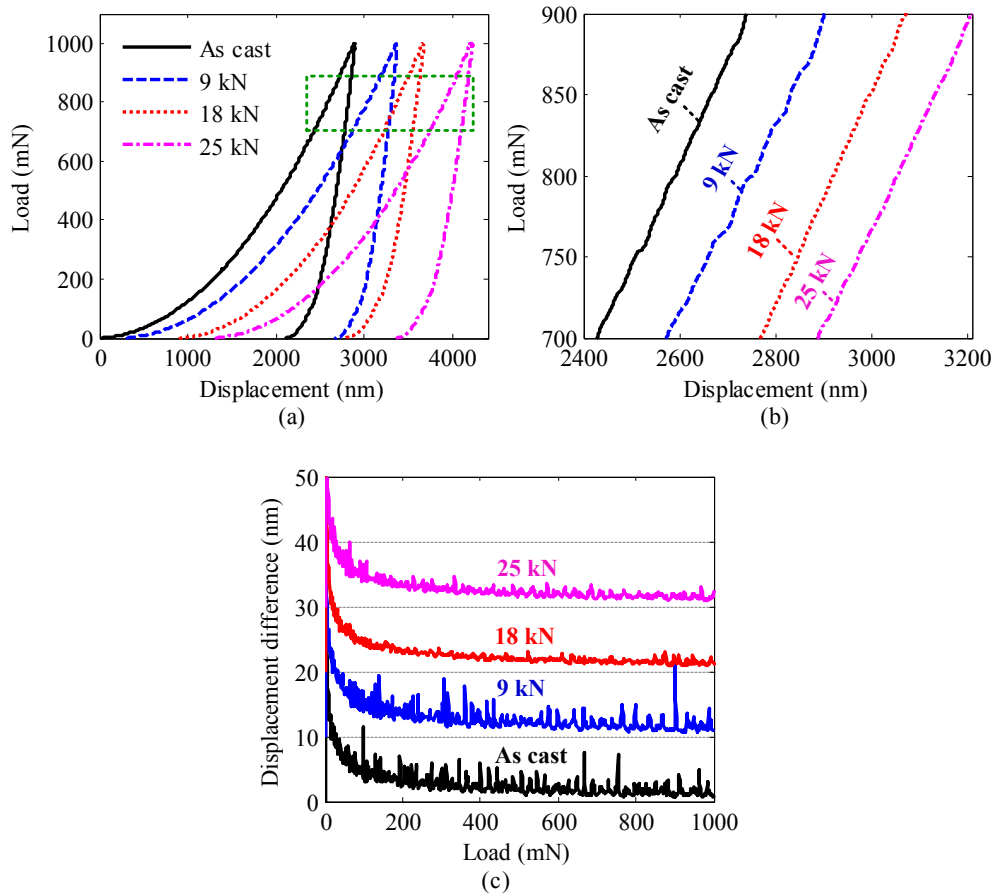
Fig. 7. (a) Load-displacement curves of the as cast and PCD samples; (b) a close view of the dotted zone in Fig. 7(a); (c) the displacement difference changing with the load for these four samples.

18 kN to 25 kN. This huge change in angle of main shear band is derived to stimulate generation of new shear bands inside the 25 kN PCD sample. Similar to the 9 kN PCD sample, these pre-existing shear bands formed during the 25 kN PCD also contributed to the subsequent plastic deformation during nano-indentation. Thus, some similar indentation behaviors to those of the 9 kN PCD sample, typically, a lower but wider pile-up (compared to that of the 18 kN PCD sample), appear for the 25 kN PCD sample.

With regard to the transition from serrated to non-serrated flows in 9 kN and 18 kN PCD samples, it may be related to the velocity relationship between the shear-band propagation and applied strain [2,30]. When the applied strain velocity overwhelms the shear-band velocity of a single band, non-serrated flows will be observed. From this perspective, different serrated flows shown in Fig. 7 suggest different dynamics of shear-band propagation because they have the same experimental conditions. Promoted serrated flows in the 9 kN PCD sample may denote a larger shear-band propagation velocity because shear bands can directly propagate from these pre-existing shear bands, while PCD with a 18 kN load lowers the shear-band propagation velocity, probably because of the dominated factor of compressive residual stress.

4. Conclusions

In summary, nanoindentation behaviors of $Zr_{65}Cu_{15}Al_{10}Ni_{10}$ bulk metallic glasses before and after pre-compression deformation (PCD) were comparatively investigated. Nanoindentation hardness was found to initially decrease for a 9 kN PCD sample, and then increase with the PCD load increasing to 18 kN and 25 kN. Hardness mapping indicated that PCD changed the mechanical heterogeneity, i.e., distribution of soft and hard regions. Residual morphologies and load-displacement curves of these samples were observed and analyzed. It was found that relatively smooth indent, largest pile-up width, smallest pile-up height, but promoted serrated flows were induced for the 9 kN PCD sample, suggesting a continuous plastic flow on the top surface. In contrast, 18 kN PCD induced conspicuous macroscopic shear bands, smallest pile-up width, largest pile-up height, but weakest serrated flows, suggesting highly localized plastic flow on the top surface of the 18 kN PCD sample. A competing mechanism between shear bands and compressive residual stress was adopted to rationalize these phenomena.

References

[1] C.A. Schuh, T.C. Hufnagel, U. Ramamurty, Overview No.144-mechanical behavior of amorphous alloys, Acta Mater 55 (2007) 4067–4109.

[2] R. Maass, J.F. Loffler, Shear-band dynamics in metallic glasses, Adv. Funct. Mater 25 (2015) 2353—2368.

[3] F. Szuecs, C.P. Kim, W.L. Johnson, Mechanical properties of Zr56.2Ti13.8Nb5.0Cu6.9Ni5.6Be12.5 ductile phase reinforced bulk metallic glass composite, Acta Mater 49 (2001) 1507—1513.

[4] M.M. Trexler, N.N. Thadhani, Mechanical properties of bulk metallic glasses, Prog. Mater. Sci. 55 (2010) 759—839.

[5] J. Plummer, W.L. Johnson, Is metallic glass poised to come of age? Nat. Mater 14 (2015) 553—555.

[6] S. Nachum, A.L. Greer, Indentation size effect in metallic glasses: mean pressure at the initiation of plastic flow, J. Alloy. Compd. 615 (2014) S98—S101.

[7] F.C. Li, J. Gu, M. Song, S. Ni, S.F. Guo, The evolution of local mechanical properties of bulk metallic glasses caused by structural inhomogeneity, J. Alloy. Compd. 591 (2014) 315—319.

[8] B.G. Yoo, Y.J. Kim, J.H. Oh, U. Ramamurty, J.I. Jang, On the hardness of shear bands in amorphous alloys, Scr. Mater. 61 (2009) 951—954.

[9] R. Maass, K. Samwer, W. Arnold, C.A. Volkert, A single shear band in a metallic glass: local core and wide soft zone, Appl. Phys. Lett. 105 (2014) 171902.

[10] Y.H. Chen, J.C. Huang, L. Wang, T.G. Nieh, Effect of residual stresses on nanoindentation creep behavior of Zr-based bulk metallic glasses, Intermetallics 41 (2013) 58—62.

[11] P.F. Yu, S.D. Feng, G.S. Xu, X.L. Guo, Y.Y. Wang, W. Zhao, L. Qi, G. Li, P.K. Liaw, R.P. Liu, Room-temperature creep resistance of Co-based metallic glasses, Scr. Mater. 90—91 (2014) 45—48.

[12] R. Bhowmick, R. Raghavan, K. Chattopadhyay, U. Ramamurty, Plastic flow softening in a bulk metallic glass, Acta Mater 54 (2006) 4221—4228.

[13] Y.J. Huang, B.J. Zhou, Y.L. Chiu, H.B. Fan, D.J. Wang, J.F. Sun, J. Shen, The structural relaxation effect on the nanomechanical properties of a Ti-based bulk metallic glass, J. Alloy. Compd. 608 (2014) 148—152.

[14] F.C. Li, M. Song, S. Ni, S.F. Guo, X.Z. Liao, Correlation between hardness and shear banding of metallic glasses under nanoindentation, Mat. Sci. Eng. A-Struct 657 (2016) 38—42.

[15] C.A. Schuh, T.G. Nieh, A nanoindentation study of serrated flow in bulk metallic glasses, Acta Mater. 51 (2003) 87—99.

[16] Y.I. Golovin, V.I. Ivolgin, V.A. Khonik, K. Kitagawa, A.I. Tyurin, Serrated plastic flow during nanoindentation of a bulk metallic glass, Scr. Mater. 45 (2001) 947—952.

[17] H. Huang, H. Zhao, Indenter geometry affecting indentation behaviors of the Zr-based bulk metallic glass, Mater. Trans. 55 (2014) 1400—1404.

[18] B.G. Yoo, J.Y. Kim, J.I. Jang, Influence of indenter geometry on the deformation behavior of Zr60Cu30Al10 bulk metallic glass during nanoindentation, Mater. Trans. 48 (2007) 1765—1769.

[19] F. Haag, D. Beitelschmidt, J. Eckert, K. Durst, Influences of residual stresses on the serrated flow in bulk metallic glass under elastostatic four-point bending - a nanoindentation and atomic force microscopy study, Acta Mater. 70 (2014) 188—197.

[20] W.H. Jiang, M. Atzmon, Room-temperature flow in a metallic glass - strain-rate dependence of shear-band behavior, J. Alloy. Compd. 509 (2011) 7395—7399.

[21] L. Wang, L. Wang, Y.F. Xue, H.F. Zhang, H.M. Fu, Nanoindentation response of laser shock peened Ti-based bulk metallic glass, Aip Adv. 5 (2015) 057156.

[22] M. Stolpe, J.J. Kruzic, R. Busch, Evolution of shear bands, free volume and hardness during cold rolling of a Zr-based bulk metallic glass, Acta Mater. 64 (2014) 231—240.

[23] W.H. Jiang, F.E. Pinkerton, M. Atzmon, Mechanical behavior of shear bands and the effect of their relaxation in a rolled amorphous Al-based alloy, Acta Mater. 53 (2005) 3469—3477.

[24] W.C. Oliver, G.M. Pharr, Measurement of hardness and elastic modulus by instrumented indentation: advances in understanding and refinements to methodology, J. Mater. Res. 19 (2004) 3—20.

[25] H. Bei, S. Xie, E.P. George, Softening caused by profuse shear banding in a bulk metallic glass, Phys. Rev. Lett. 96 (2006) 105503.

[26] L. Wang, H. Bei, Y.F. Gao, Z.P. Lu, T.G. Nieh, Effect of residual stresses on the hardness of bulk metallic glasses, Acta Mater. 59 (2011) 2858—2864.

[27] J.G. Wang, D.Q. Zhao, M.X. Pan, C.H. Shek, W.H. Wang, Mechanical heterogeneity and mechanism of plasticity in metallic glasses, Appl. Phys. Lett. 94 (2009) 031904.

[28] A. Bolshakov, G.M. Pharr, Influences of pileup on the measurement of mechanical properties by load and depth sensing indentation techniques, J. Mater. Res. 13 (1998) 1049—1058.

[29] H. Huang, H.W. Zhao, Z.Y. Zhang, Z.J. Yang, Z.C. Ma, Influences of sample preparation on nanoindentation behavior of a Zr-based bulk metallic glass, Materials 5 (2012) 1033—1039.

[30] R. Maass, D. Klaumunzer, J.F. Loffler, Propagation dynamics of individual shear bands during inhomogeneous flow in a Zr-based bulk metallic glass, Acta Mater. 59 (2011) 3205—3213.